Journal of Colloid and Interface Science 501 (2017) 112–122

Contents lists available at ScienceDirect

Journal of Colloid and Interface Science

journal homepage: www.elsevier.com/locate/jcis

Regular Article

Structure and dynamics of cetyltrimethylammonium chloride-sodium dodecylsulfate (CTAC-SDS) catanionic vesicles: High-value nano-vehicles from low-cost surfactants

Irene Russo Krauss [a,b], Riccardo Imperatore [a,b], Augusta De Santis [a,b], Alessandra Luchini [a,b,c], Luigi Paduano [a,b], Gerardino D'Errico [a,b,*]

[a] Department of Chemical Sciences, University of Naples "Federico II", Complesso di Monte S. Angelo, Via Cinthia, I-80126 Naples, Italy
[b] CSGI (Consorzio per lo Sviluppo dei Sistemi a Grande Interfase), via della Lastruccia 3, I-50019 Florence, Italy
[c] Institut Laue-Langevin, BP 156, 71 Avenue des Martyrs, 38000 Grenoble, France

GRAPHICAL ABSTRACT

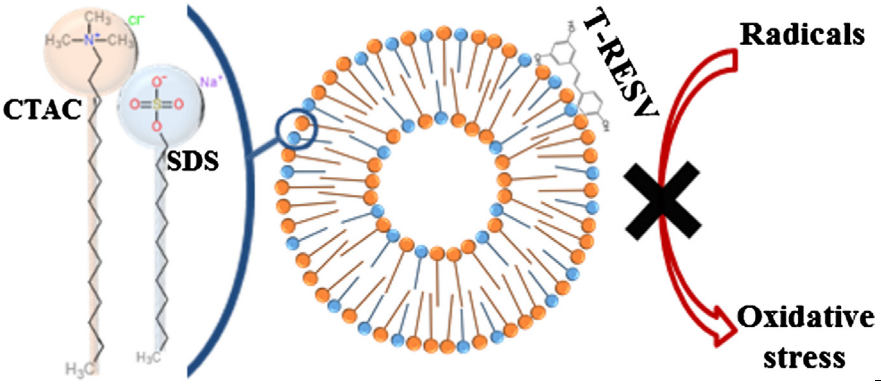

ARTICLE INFO

Article history:
Received 31 January 2017
Revised 9 April 2017
Accepted 10 April 2017
Available online 12 April 2017

Keywords:
Catanionic vesicles
Phase diagram
Drug carrier
Solubilization
Resveratrol

ABSTRACT

Hypothesis: Catanionic vesicles based on large-scale produced surfactants represent a promising platform for the design of innovative, effective and relatively inexpensive nano-vehicles for a variety of actives. Structural, dynamic and functional behavior of these aggregates is finely tuned by the molecular features of their components and can be opportunely tailored for their applications as drug carriers.
Experiments: Here we investigate the aggregates formed by CTAC and SDS, two of the most diffused surfactants, by means of Dynamic Light Scattering, Small Angle Neutron Scattering and Electron Paramagnetic Resonance spectroscopy (EPR). The exploitation of these aggregates as nano-vehicles is explored using the poorly water-soluble antioxidant *trans*-resveratrol (*t*-RESV), testing *t*-RESV solubility and antioxidant activity by means of UV, fluorescence spectroscopy and EPR.
Findings: The presence of a large stability region of catanionic vesicles on the CTAC-rich side of the phase diagram is highlighted and interpreted in terms of the mismatch between the lengths of the surfactant tails and of first reported effects of the chloride counterions. CTAC-SDS vesicles massively solubilize *t*-RESV, which in catanionic vesicles exerts a potent antioxidant and radical-scavenging activity. This behavior arises from the positioning of the active at the surface of the vesicular aggregates thus being sufficiently exposed to the external medium.

* Corresponding author.
E-mail address: gerardino.derrico@unina.it (G. D'Errico).

http://dx.doi.org/10.1016/j.jcis.2017.04.032
0021-9797/

1. Introduction

Aqueous mixtures of oppositely charged surfactants, i.e. catanionics, spontaneously form a variety of supramolecular aggregates [1–7] whose structural, dynamic and functional features are finely tuned by a combination of factors, including molecular architecture of the surfactants (e.g., headgroup bulkiness and charge density [8], tail length and branching [9]), mixture composition and total surfactant concentration [10], presence of additives (organic substances and/or electrolytes), temperature [11]. At relatively low surfactant concentration, either wormlike micelles or vesicles form. Both kinds of aggregates present a high technological potential, as wormlike micelles can be used to tune the viscoelastic behavior of the mixtures [12,13], while vesicles can be used in drug delivery [14]. Particularly, catanionic vesicles have been proposed for various pharmaceutical applications [15–17]. With respect to conventional liposomes, they possess higher kinetic stability and can be prepared in much easier and cheaper ways [18,19].

In most of the studies concerning catanionic mixtures, alkylammonium bromides surfactants are chosen as positively charged components [20,21]; at the same time, dichained species are often chosen [22,23]. Mixtures including single-chained ammonium chlorides have been much less investigated [24]. In this work we focus on the supramolecular aggregates formed by cetyltrimethylammonium chloride (CTAC, IUPAC name hexadecyltrimethylammonium chloride) and sodium dodecylsulfate (SDS) in aqueous mixtures. Their behavior is of large basic interest, considering that the effect of the counterion, and specifically of the naturally abundant chloride, on the features of catanionic aggregates is still not completely understood. Despite cetyltrimetylammonium and dodecylsulfate species represent a sort of reference in the study of cationic and anionic surfactants, respectively, CTAC-SDS aqueous mixtures have never been investigated experimentally, while a computational analysis of the supramolecular aggregates formed in this system, based on coarse-grained molecular dynamics simulations, has been recently published [25]. Our study offers an opportunity to provide an experimental support to computational results.

The present study also has an applicative interest. Chloride is the counterion of choice for cationic surfactants in most of their practical applications (e.g., as fabric softeners [26], sanitizers/disinfectants [27]). Specifically, CTAC is largely used in personal care products, thus the design, preparation and characterization of CTAC-based catanionic vesicles, suitable for the solubilization of actives (antioxidants, vitamins, peptides, enzymes), would pave the way to a new generation of cosmeceutics, the hybrid category of products between pharmaceuticals and cosmetics [28].

Here, we present the chemico-physical characterization of the ternary system water-CTAC-SDS through the determination and analysis of the phase diagram, obtained by means of Dynamic Light Scattering (DLS). The aggregate structure and dynamics is deeply analyzed by Small Angle Neutron Scattering (SANS) and Electron Paramagnetic Resonance spectroscopy (EPR).

We also explore the suitability of CTAC-SDS supramolecular aggregates as nano-vehicles. To this purpose we have chosen *trans*-resveratrol (3,5,4′-trihydroxy-*trans*-stilbene, *t*-RESV), a natural polyphenol that has a strong antioxidant activity [29,30], whose practical application is limited by the poor water solubility, that in turn leads to low bioavailability, and by the chemical instability. Several different nano-vehicles have been proposed for *t*-RESV solubilization [31–35], but applications of ionic surfactants for the same purpose remain unexplored. The large availability of these species, and the relative inexpensiveness of the derived nano-vehicles would tremendously favor exploitation of *t*-RESV or similar antioxidants. We quantitatively assess the *t*-RESV solubilization capacity of different CTAC-SDS supramolecular aggregates by means of UV spectroscopy, identifying the active positioning with respect to the surfactant molecules by spectrofluorimetry. Finally, we test the radical scavenging activity of *t*-RESV, when incorporated into these nano-vehicles, by EPR measurements. To this aim, we propose an innovative method, designed to monitor the effectiveness of antioxidant actives in the aqueous medium surrounding surfactant aggregates.

2. Materials and methods

2.1. Materials and sample preparation

SDS, CTAC, 4-hydroxy-2,2,6,6-tetramethylpiperidin-1-oxyl (TEMPOL) and 5-DOXYL-stearic acid (5-DSA) of high purity were purchased from Sigma Aldrich (St. Louis, MO, USA). *t*-RESV was purchased by Fagron-Italia (Bologna, Italy). All materials were used without further purification. Ultra-high-quality water (resistivity = 18.2 MΩ cm; EMD Millipore, Billerica, MA, USA) was used for preparation of all samples, with the only exception of samples for SANS measurements, for which D_2O (purchased from Sigma Aldrich, isotropic enrichment >99.8%) was used. All surfactant mixtures were prepared by proper mixing/dilution of two stock concentrated solutions of CTAC and SDS at 0.0625 and 0.41 mol kg^{-1}, respectively. Samples at total surfactant concentration 0.01, 0.02 and 0.03 mol kg^{-1} and with different molar ratios of anionic/cationic surfactants were prepared. Please note that in the following the compositions of CTAC-SDS mixtures are always reported as molar ratios. In all cases, a 5 min strong agitation of the samples was applied by using a vortexer to promote mixing of the surfactants.

2.2. Dynamic light scattering measurements

DLS measurements were performed with a home-made instrument composed of a Photocor compact goniometer, a SMD 6000 Laser Quantum 50 mW light source operating at 5325 Å, a photomultiplier (PMT-120-OP/B) and a correlator (Flex02-01D) from *Correlator.com*. The experiments were carried out at the constant temperature (25.0 ± 0.1) °C, by using a thermostatic bath, and at the scattering angle θ of 90°. The scattered intensity correlation function was analyzed using a regularization algorithm [36]. The diffusion coefficient of each population of diffusing particles was calculated as the z-average of the diffusion coefficients of the corresponding distributions [37]. Considering that the mixtures are dilute, the Stokes–Einstein equation was used to evaluate the hydrodynamic radius, R_H, of the aggregates from their translation diffusion coefficient, *D*. Samples were monitored for two months to check their stability.

2.3. Electrophoretic light scattering measurements

Zeta potential of CTAC-SDS aggregates was assessed by means of electrophoretic light scattering (ELS), by using a Zetasizer Nano ZSP (Malvern Instruments, England). The measurements were performed using 0.03 mol kg^{-1} mixtures in pure water and polystyrene Folded Capillary Zeta cells (Malvern Instruments). Each measurement was performed at 25 °C upon 90 s equilibration time. For zeta potential determination, the average of three measurements has been taken.

2.4. Small angle neutron scattering measurements

SANS measurements for pure surfactant systems and for 70:30 CTAC-SDS vesicles were performed with the LOQ small angle diffractometer at ISIS Pulsed Neutron Source (Science and

Technology Facilities Council, Rutherford Appleton Laboratory, Didcot - UK) [38]. The instrument is characterized by a fixed two-dimensional detector positioned at 4 m from the sample, which can detect the position and time of arrival of the scattered neutrons. This configuration allowed collecting data in a range of the scattering vector modulus $q = 4\pi/\lambda \sin(\theta/2)$ between 0.006 $Å^{-1}$ and 0.24 $Å^{-1}$, where θ is the scattering angle and λ the neutron wavelength. Instrument resolution is 5 mm. Measurements for 30:70 CTAC-SDS vesicles were performed with the KWS2 instrument located at the Heinz Meier Leibtnitz Source, Garching Forschungszentrum (Germany) [39]. Neutrons with a wavelength spread $\Delta\lambda/\lambda \leqslant 0.2$ were used. A two-dimensional array detector at different wavelength, collimation, sample-to-detector distance combinations measured neutrons scattered from the samples. We chose configurations that allowed collecting data in a range of q between 0.008 $Å^{-1}$ and 0.279 $Å^{-1}$.

The samples were contained in a closed quartz cell, in order to prevent the solvent evaporation, and all measurements were performed at 25 °C. Each measurement lasted for a period sufficient to obtain ~2 million counts. The raw data were corrected for background and empty cell scattering. Detector efficiency correction, radial average and transformation to absolute scattering cross sections $d\Sigma/d\Omega$ were made with a secondary plexiglass standard [40,41]. The absolute scattering cross section data $d\Sigma/d\Omega$ were plotted as function of q. The dependence of $d\Sigma/d\Omega$ from the scattering vector can summarized as shown in Eq. (1):

$$\frac{d\Sigma}{d\Omega} = n_p P(q) S(q) + \left(\frac{d\Sigma}{d\Omega}\right)_{incoh} \quad (1)$$

where n_p is the number of scattering objects, $P(q)$ and $S(q)$ are respectively the form factor and the structure factor. The last term takes into account the incoherent scattering mostly due to the presence of hydrogen atoms within the sample. Structural information can be extrapolated by choosing an appropriate model to fit the experimental data. In the case of catanionic vesicles, only a form factor has been taken into account, while for pure CTAC and SDS mixtures also a structure factor was considered in the fitting procedure, as detailed in the Results and Discussion section.

2.5. Electron paramagnetic resonance measurements

For the EPR characterization of the CTAC-SDS aggregates, 5-DSA was introduced in the mixtures as spin probe, because it is a surfactant able to co-aggregate with CTAC and/or SDS. Spin labelled samples were prepared as follows: a small aliquot of 5-DSA in ethanol at 1 mg ml^{-1} was poured in a vial; a thin film was produced by evaporating the solvent with dry nitrogen gas and final traces of solvent were removed by subjecting the sample to vacuum desiccation for at least 3 h; then the probe film was hydrated with the surfactant mixture and incubated for 10 min. EPR spectra were recorded on a 9 GHz Bruker Elexys E-500 spectrometer (Bruker, Rheinstetten, Germany). Capillaries filled with 20 µl of samples and sealed were placed in a standard 4 mm quartz tube, also containing light silicone oil to assure thermal stability. The temperature of the sample was kept constant at 25 °C during the measurements. Instrumental settings were as follows: sweep width 100 G; resolution 1024 points; modulation frequency 100 kHz; modulation amplitude 1.0 G; time constant 20.5 ms, incident power 6.4 mW, gain 60 dB. With the aim to improve the signal-to-noise ratio, 16 scans were accumulated in all the cases.

EPR simulations were performed using computer software freely available on the anonymous FTP server at the Illinois EPR Research Center [42], modified to include routines for automatic least-squares fitting (Simplex and Levenberg-Marquardt methods) [43]. The simulation procedure is detailed in previous works [44,45].

2.6. Preparation of t-RESV containing samples

Samples of *t*-RESV in the presence of the different surfactant self-aggregates were prepared by adding an excess amount of *t*-RESV to 2 g of the aqueous surfactant mixtures. The total surfactant molality ranged from 0 to 0.03 mol kg^{-1}. The samples were shaken for 24 h in a thermostated bath at 25 °C. In order to minimize photochemical degradation of *t*-RESV, all vials were covered with aluminum foil. Once equilibrium was reached, suspensions were kept at rest for 1 h, after which undissolved *t*-RESV powder settled at the vial bottom. The supernatants were separated, opportunely diluted and finally analyzed by UV spectroscopy. The procedure did not include a filtration or centrifugation step, to avoid possible perturbation and/or partial separation of the surfactant aggregates.

For determination of scavenging capacity of *t*-RESV, surfactant mixtures at constant total surfactant concentration (0.03 mol kg^{-1}) were prepared using a diluted TEMPOL solution (10^{-4} M) as solvent. Two sets of samples were prepared. In the former one, an excess of *t*-RESV was added to the surfactant solutions; each sample was incubated at 37 °C for 1 h, and then the supernatant was analyzed. In the latter set of samples, an equal *t*-RESV amount was added to the various surfactant solutions (0.0015 mol kg^{-1}).

2.7. UV–Vis measurements

t-RESV solubility in CTAC and SDS micelles, as well as in CTAC-SDS vesicles at 70:30 and 30:70 ratio, was evaluated determining the concentration of *t*-RESV in the different mixtures by means of UV spectroscopy [46]. Spectra were collected at 25 °C on a Jasco 530 UV–Vis spectrophotometer (Jasco Inc., Easton, MD), in the 500–220 nm range, with a band width of 1 nm, scanning speed of 200 nm min^{-1} and using a 0.1 cm path length of the cell. Each experiment was repeated thrice.

With the aim to obtain a careful determination of *t*-RESV concentration in the different samples, we preliminarily determined the molar extinction coefficient of *t*-RESV in CTAC and SDS mixtures at λ = 326 nm. They are scarcely sensitive to the presence of surfactants (see the Supporting information for details, and Table S1), so that in all systems we used the average value 29,500 ± 1500 M^{-1} cm^{-1}.

2.8. Fluorescence measurements

t-RESV fluorescence spectra in different solution conditions (i.e. in the presence of CTAC micelles, SDS micelles, mixed catanionic vesicles and in water) were recorded with a JASCO FP-750 spectrofluorometer using a 1 cm path length of the cell, at 25 °C. *t*-RESV was excited at 318 nm and the emission was recorded from 330 to 500 nm at a scanning speed of 250 nm min^{-1}, with a 5 nm emission slit width, and corrected for background signal.

2.9. Determination of t-RESV scavenging capacity

The scavenging capacity of *t*-RESV against the stable water-soluble free radical TEMPOL was evaluated in CTAC and SDS micelles, as well as in CTAC-SDS vesicles at 70:30 and 30:70, by monitoring the decreasing of TEMPOL signal through EPR measurements. A procedure previously used for the determination of the scavenging activity of antioxidants contained in foods and drinks was purposely modified and adapted [47,48]. In particular, the use of ethanol or other compounds that could alter *t*-RESV solubility and nano-vehicles structural properties was carefully avoided. Two sets of samples containing *t*-RESV, TEMPOL and surfactants,

prepared as previously described, were analyzed by EPR, using the same experimental settings reported above. The intensity of the TEMPOL signal, a well-defined triplet, was measured as the peak-to-peak height of the second line. The scavenging activity of *t*-RESV was defined as $(h_0 - h_x)/h_0 \times 100$, where h_0 and h_x are the height of the second line in the EPR spectrum of TEMPOL in the absence and in the presence of the different antioxidant nanovehicles, respectively.

3. Results and discussion

3.1. CTAC-SDS-water phase diagram

The ternary phase diagram of the diluted CTAC-SDS-water system at 25 °C is shown in Fig. 1.

Both binary systems present an isotropic micellar phase; the critical micelle concentration (cmc) values, as reported in the literature [49,50], are quoted in the diagram and in Supplementary Fig. S1 as well as reported in Table 1. The blue dotted-dashed line indicates the CTAC-SDS equimolar ratio; samples lying above the line present an excess of CTAC, whereas the ones lying below have an excess of SDS. The distinction between different structures of the surfactant supramolecular aggregates (micelles *vs.* vesicles) and the identification of the phase diagram areas where these structures form have been obtained by DLS, SANS and EPR measurements [51], as detailed in the next subsection. The green, red and black dots indicate the mixtures at 0.01, 0.02 and 0.03 mol kg^{-1} total surfactant concentration, respectively, which have been prepared and analyzed in details.

Even in the considered high dilution region, the existence of different phases is observed, both as single phases and as biphasic equilibrium mixtures. In equimolar mixtures of the two surfactants, a catanionic precipitate forms. Moving from the equimolar line towards the CTAC or SDS binary system sides, a qualitatively similar phase behavior is observed. Upon addition of either one of the two surfactants, the catanionic precipitate dissolves and a bluish vesicular suspension forms. Further addition of surfactants results in the formation of mixed micelles, whose stability region extends close to the axes representing the binary systems. On the SDS-rich side of the diagram, a region in which vesicles and micelles coexist is clearly detectable.

Overall, the system behavior is in good agreement with results obtained for similar ternary mixtures [4]. However, some specific features deserve additional comments. The region in which precipitate forms, close to the equimolarity line, is very narrow. This is related to the different length of the surfactant tails, which favors the formation of curved bilayers, thus resulting in wide regions of vesicle stability [5]. Indeed, catanionic mixtures of single-chained surfactants with the same chain length present a much wider region in which precipitation occurs [24]. Because of the strong synergistic effects of the two oppositely charged surfactants, vesicles start to form at very low total surfactant concentration, as proved by the values of critical aggregation concentration (cac) of the two catanionic mixtures CTAC-SDS 70:30 and 30:70, determined by surface tension measurements (see Supporting Information, Fig. S2) and reported in Table 1. In both cases, the cac's are much lower than the cmc's of pure surfactants (see Supporting Information, Fig. S1).

Interestingly, a region where vesicles and micelles coexist is identified only on the SDS-rich side of the diagram, while on the CTAC-rich side vesicle formation is predominant. This behavior differs from what reported in the literature for similar ternary systems, all showing a detectable coexisting region on the cationic side [20–23], or the prevalence of micellar aggregates [52]. Since

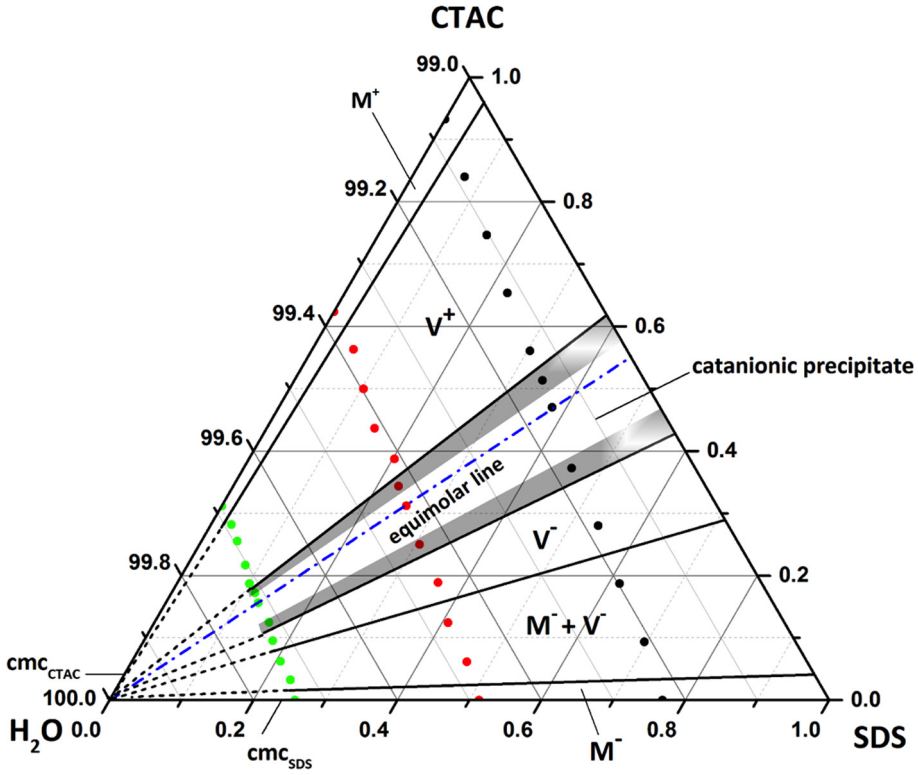

Fig. 1. Partial phase diagram of the ternary system CTAC-SDS-water at 25 °C. Concentrations reported on the three axes are intended as weight percentages. Experimental points are marked with dots. The catanionic precipitate region is marked explicitly; M^+ and M^- indicate cationic and anionic micelles, respectively; V^+ and V^- indicate cationic and anionic vesicles, respectively; $M^- + V^-$ indicates the multiphase region where anionic micelles and vesicles coexist. The cmc values for SDS and CTAC are marked on the corresponding axes.

Table 1
Critical aggregation concentration, mean hydrodynamic radius and structural features of CTAC or/and SDS self-aggregates in aqueous mixtures at 0.03 mol kg^{-1} total surfactant concentration, as determined by different experimental techniques.

	cmc/cac (mol kg^{-1}) Surface tension	R_H (nm) DLS	Aggregate type DLS SANS	Charge SANS	Semiminor axis (nm) SANS	Semimajor axis (nm) SANS	Bilayer thickness (nm) SANS
SDS	9.5×10^{-3}[a]	2.1 ± 0.5	Prolate micelles	9	1.6 ± 0.1	3.3 ± 0.1	–
CTAC	1.1×10^{-3}[b]	2.2 ± 0.5	Prolate micelles	22	2.1 ± 0.1	3.5 ± 0.1	–
CTAC-SDS 30:70 mol/mol	1.8×10^{-4}	61 ± 2	Unilamellar vesicles	–	–	–	3.6 ± 0.2
CTAC-SDS 70:30 mol/mol	2.7×10^{-5}	60 ± 3	Unilamellar vesicles	–	–	–	3.3 ± 0.1

[a] From Ref. [49].
[b] From Ref. [50].

catanionic mixtures including CTAB (cetyltrimethylammonium bromide) in the formulation also present an extended composition range in which vesicles and micelles coexist [20,21], a main role in determining vesicle stability in CTAC-containing mixtures is likely to be played by the chloride counterion.

In aqueous solutions of pure cationic surfactants, changing the counterion from bromide to chloride causes a counterion binding decrease and a cmc increase [53]. This is due to the smaller size of the chloride ion, which makes it more strongly hydrated. Strongly hydrated ions are less prone to adsorb on the surface of the micelles, thus increasing the charge repulsion between the positive headgroups and disfavoring self-aggregation [53]. These considerations hold also for mixed micellar aggregates with a large excess of cationic surfactants [52]. Moreover, lower counterion binding, increasing the spontaneous curvature of the aggregate interface, also results in a lower tendency for the system to form bilayer aggregates, so that in principle vesicle formation should be even more disfavored with respect to micellization [5]. In contrast, our results show that the chloride counterions stabilize positively charged catanionic vesicles with respect to micellar aggregates. To the best of our knowledge, this is the first case in which this effect is reported. It is to be considered that in catanionic vesicles ion pairing between the oppositely charged headgroups of the two surfactants reduces the need of counterion condensation, so that any effect of the counterion nature on the aggregate structure is deadened, with respect to what observed for micelles [52]. Moreover, surfactant ion pairs do not pack favorably into globular micelles. Instead, they prefer to assemble into bilayer-based structures, with low curvature, such as vesicles [5]. As a result, vesicles are favored with respect to micelles, and the diagram region in which only vesicles are present significantly extends.

A recent computational investigation by Wang et al. on the CTAC-SDS aqueous mixtures [25] also helps to understand why, on the CTAC-rich side of the diagram, catanionic vesicles are preferred to micellar aggregates, while on the SDS-rich side micelles co-exist with vesicular aggregates. According to these authors, CTAC-SDS mixed micelles tend to assume a disk-like shape, with the surfactant ion pairs occupying the planar part of the aggregates while the surfactant in excess would concentrate at the border. Now, we have to consider that in anionic-rich aggregates, SDS has a relatively short chain so that it can self-organize at the disk-shaped micelle border in order to shield the aggregate interior from the contact with water molecules. In contrast, in cationic-rich aggregates, excess CTAC molecules are not able to do the same, thus destabilizing micellar aggregates and favoring vesicles formation, in line with our experimental results.

3.2. Structural and dynamical characterization of CTAC-SDS aggregates

Identification of surfactant aggregate morphology was initially based on DLS measurements. This analysis allowed the detection of the number of different populations of aggregates present in each sample and, on the basis of the mean hydrodynamic radius, to discriminate between micelles and vesicles. Representative mean hydrodynamic radii evaluated from these measurements are collected in Table 1, while some examples of the aggregate distributions as obtained by DLS for several mixtures at 0.03 mol kg^{-1} concentration are reported in Fig. 2(a). Inspection of the figure shows that for pure surfactants small aggregates are found, which can be identified as micelles, whereas in mixed systems larger aggregates are observed, which may be reasonably recognized as catanionic vesicles. These vesicles coexist with micelles in the CTAC-SDS 10:90 mixture.

Analysis of the samples at lower total surfactant concentration (0.01 and 0.02 mol kg^{-1}) gave similar results. On both the cationic- and the anionic-rich side, vesicle dimension at a given CTAC-SDS ratio is only slightly affected by the total surfactant concentration (data not shown). However, in the cationic rich side, the stability domain of the vesicular aggregates is large enough to analyze the dependence of the aggregate dimension on the CTAC-SDS ratio (see Fig. 2(b)).

Irrespective of the surfactant concentration, the maximum radius of the vesicles (corresponding to the minimum curvature of their surface) is reached at CTAC-SDS 80:20 ratio. At higher ratios, the surfactant packing is hindered by the electrostatic repulsion between the excess of positively charged CTAC head groups. At lower ratios, the mismatching between the tail length of CTAC and SDS disturbs self-organization of surfactants. These observations confirm that the key factors that modulate the morphology of CTAC-SDS vesicles are the repulsion between the charged headgroups, partially screened by the counterions, and the different length of the surfactant acyl chain. All samples were monitored by DLS for two months, and no change in the aggregate dimension was found.

The zeta potential, reflecting the surface charge, has been evaluated by means of ELS for the different CTAC-SDS aggregates. As clearly emerges from Fig. 2(c), SDS rich aggregates are characterized by a negative zeta potential, slightly lower for micelles with respect to vesicles (−63 vs −54 mV for SDS micelles and CTAC-SDS 30:70 vesicles, respectively). Beyond the catanionic precipitate range, CTAC rich aggregates are characterized by an almost opposite zeta potential value, ranging from 55 mV of 70:30 vesicles to 71 mV of pure CTAC micelles.

A deeper insight into the structural features of surfactant aggregates can be obtained by means of SANS. In the case of CTAC-water and SDS-water systems, SANS profiles (Fig. S3) clearly show the presence of a peak due to electrostatic interparticle interaction. So the contribution of a structure factor was taken into account, in addition to the form factor, to fit the data. In both cases the scattered intensity was fitted considering the micelles as interacting charged ellipsoids and using the Hayter and Penfold model for the structure factor [54]. Structural features determined by fitting experimental data are summarized in Table 1. Micelle dimensions well agree with literature values, [55–57] as well as the counterion

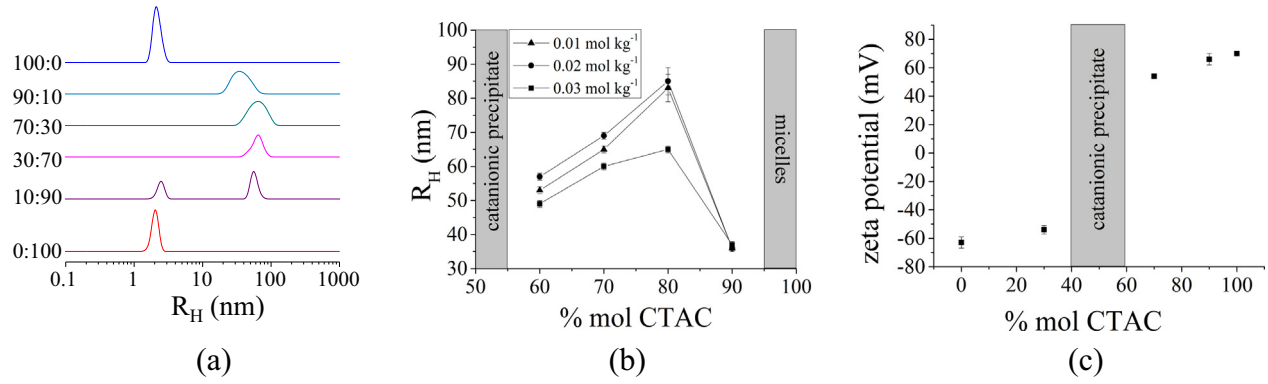

Fig. 2. (a) Intensity weighed hydrodynamic radius distributions of CTAC-SDS aggregates at 0.03 mol kg^{-1} total surfactant concentration and various CTAC:SDS molar ratios. (b) Variation of the mean hydrodynamic radius of CTAC-rich CTAC-SDS vesicles, as determined by DLS, as a function of the surfactant composition at three different total surfactant concentrations. (c) Zeta potential values of CTAC-SDS aggregates at 0.03 mol kg^{-1} total surfactant concentration and various CTAC:SDS molar ratios.

condensation percentage, as calculated from the micelle charge obtained by SANS fitting, that is 72% and 83% for CTAC and SDS micelles, respectively.

For what concerns the CTAC-SDS catanionic aggregates at 70:30 and 30:70 ratio, SANS profiles are reported in Fig. 3: a predominant form factor characterizes both scattering profiles, with no peak due to electrostatic interparticle interaction. For this reason, no structure factor was introduced in the model function used for the data analysis. In the low-q region (0.008–0.08 $Å^{-1}$), data display a q^{-2} decay characteristic of locally planar surfaces, thus indicating that vesicles composed by a single lamella are present in both systems.

For a vesicle geometry where the aggregate radius is much greater than the bilayer thickness, the bilayer can be modelled as an extended sheet. In the limit of $S(q) \rightarrow 1$, such as our case, the following relation is valid [58]:

$$\ln(Iq^2) = c \ln(\Delta\rho)^2 - q^2 R_t^2 \quad (2)$$

where $\Delta\rho$ is the contrast variation, c is a constant and R_t is the thickness radius of gyration. In this case the thickness δ is obtained through

$$\delta = \frac{R_t}{\sqrt{12}} \quad (3)$$

Analysis of SANS data according to this approach indicates a bilayer thickness for both 70:30 and 30:70 CTAC-SDS vesicles of about 3.4 nm. A thorough analysis was performed by fitting Eq. (1) to the experimental data, where S(q) is equal to 1 and the form factor is reported in Eq. (4) [59]

$$P(q) = 2\frac{\Delta\rho^2}{q^2}(1 - \cos(q\delta)) \quad (4)$$

$\Delta\rho$ is the difference between the scattering length density of the solvent (D_2O) and that of the vesicle lamella, while δ is the bilayer thickness. In the fitting procedure the scattering length density of the lamella was considered homogenous and calculated according to its molar composition and molecular volume as: $\rho_{CTAC\text{-}SDS\ 70:30} = -1.4 \cdot 10^{-7}\ Å^{-2}$ $\rho_{CTAC\text{-}SDS\ 30:70} = -4.2 \cdot 10^{-8}\ Å^{-2}$. Differences in the bilayer thickness ($\delta_{CTAC\text{-}SDS\ 30:70} = 3.6$ nm; $\delta_{CTAC\text{-}SDS\ 70:30} = 3.3$ nm) between the two vesicles are within the experimental error.

Considering that the length of two SDS molecules in all-*trans* conformation aligned consecutively tail-to-tail is 4.1 nm [60], and for CTAC this value is around 4.9 nm, the experimental values of the thickness of CTAC-SDS bilayers suggest that the molecules tend to assume disordered conformations. Moreover, the mismatch between the lengths of the two surfactants could favor interdigitation of the tail termini at the interface between the two surfactant leaflets composing the bilayer.

Finally, the ordering and dynamics of the surfactant molecules in the catanionic aggregates were investigated by means of EPR, using 5-DSA as a molecular probe, and compared with those observed in the micellar aggregates formed by the single surfactants. 5-DSA is an amphiphilic molecule bearing the reporter nitroxide group close to the hydrophilic head group (see the inset

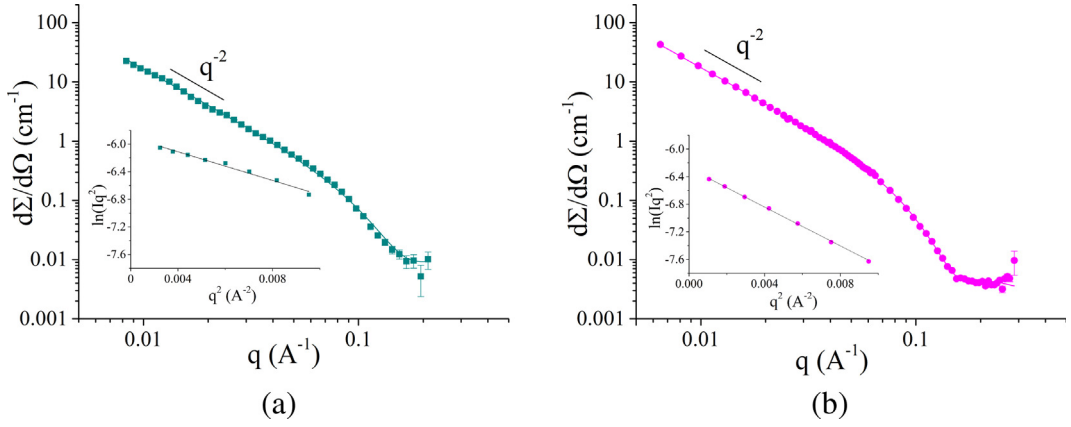

Fig. 3. Neutron scattered intensity for CTAC-SDS mixtures at 0.03 mol kg^{-1} and 70:30 (a) and 30:70 (b) ratios. Fitting curves are also reported, see text. Modified Guiner plots for flat planes are reported in the insets.

of Fig. 4). Consequently, it inserts in the surfactant aggregates monitoring the environment just underneath the interface [61,62].

In Fig. 4 the EPR spectra of 5-DSA in the aggregates formed by pure surfactants and their mixtures at 70:30 and 30:70 ratio, all at 0.03 mol kg^{-1} total surfactant concentration, are reported. In pure SDS solutions, an almost isotropic three-line shape is observed, indicating that the rotational motion of the probe is relatively unhindered, and is similar along the three molecular axes [63]. In pure CTAC solutions a similar result is observed, but the 5-DSA lines are broadened. A quantitative analysis of these spectra was performed by simulation, as detailed in the ESI (Fig. S4), obtaining the nitrogen isotropic hyperfine coupling constant (a_N) and the nitroxide correlation time (τ_C). The values of these parameters are reported in Table 2. They are in good agreement with literature data [63–65]. a_N depends on the polarity of the medium in which the nitroxide is embedded and on the formation of H-bonds involving the nitroxide group of the probe, while τ_C depends on the probe rotational mobility, as determined by the microenvironment viscosity. Inspection of Table 2 reveals that the motion of the reporter group is slowed down in the CTAC aggregates with respect to SDS ones. This indicates a more viscous microenvironment in the former type of aggregates, suggesting a tighter packing of the surfactant tails with respect to SDS micelles.

In catanionic vesicles, the 5-DSA spectra assume an anisotropic line shape, highlighted by the shoulder of the low-field maximum and the splitting of the high-field minimum (see Fig. 4). These evidences indicate that the rotational motion along the three axis is different, as expected when the probe inserts into bilayered surfactant arrangements [61], in which the motion along the direction perpendicular to the aggregate surface is different from that along the other two axes. A quantitative analysis of these spectra was realized determining, besides a_N, the order parameter, S, as reported in the literature [66]. S is a measure of the local orientational ordering of the radical group with respect to the normal to the aggregate surface. The a_N values determined for the catanionic vesicles is lower than those observed in the micellar systems, indicating that the 5-DSA reporter group experiences a more hydrophobic environment. In the catanionic vesicles the repulsions between the surfactant headgroups are minimized and the tails are more densely packed. However, the S values in the CTAC-SDS vesicles are much lower than those observed when 5-DSA is used to probe bilayers formed by typical two-tail lipids (for which values of about 0.5 are found [67]), showing a looser and more dynamic ordering of the tails with respect to lipid bilayers. This is in good agreement with SANS results discussed above.

Table 2
Spectral parameters of 5-DSA in CTAC or/and SDS aqueous mixtures at 0.03 mol kg^{-1} total surfactant concentration, as determined by EPR.

	a_N (G)	τ_C (ns)	S
SDS	15.3 ± 0.1	0.9 ± 0.1	
CTAC	15.0 ± 0.1	1.7 ± 0.2	
CTAC-SDS 30:70 mol/mol	13.4 ± 0.2		0.24 ± 0.02
CTAC-SDS 70:30 mol/mol	13.8 ± 0.2		0.30 ± 0.03

3.3. t-RESV solubilization by CTAC-SDS aqueous mixtures

The solubility of *t*-RESV (whose molecular structure is reported in the inset of Fig. 5(a)) in CTAC-SDS catanionic vesicles and, for comparison, in the micelles formed by the single surfactants, was evaluated by UV–Vis spectroscopy. The *t*-RESV spectrum in aqueous solution consists of a broad band centered around 320 nm, given by the overlapping of two peaks due to $\pi \rightarrow \pi^*$ transitions involving the benzene rings of the molecule [68]. We preliminarily tested these spectral features to be not affected by the presence of SDS and/or CTAC aggregates. The *t*-RESV molar extinction coefficient is also scarcely sensitive to the presence of surfactants (see the Supporting Information), with an average value 29,500 ± 1500 M^{-1} cm^{-1}.

To assess *t*-RESV solubility, for each surfactant system we prepared different samples with increasing surfactant concentration. All the samples were saturated with *t*-RESV, as described in the Materials and methods section, and analyzed by UV spectroscopy. In all the cases, spectral features typical of resveratrol in the *trans* configuration were observed, thus assuring that no isomerization

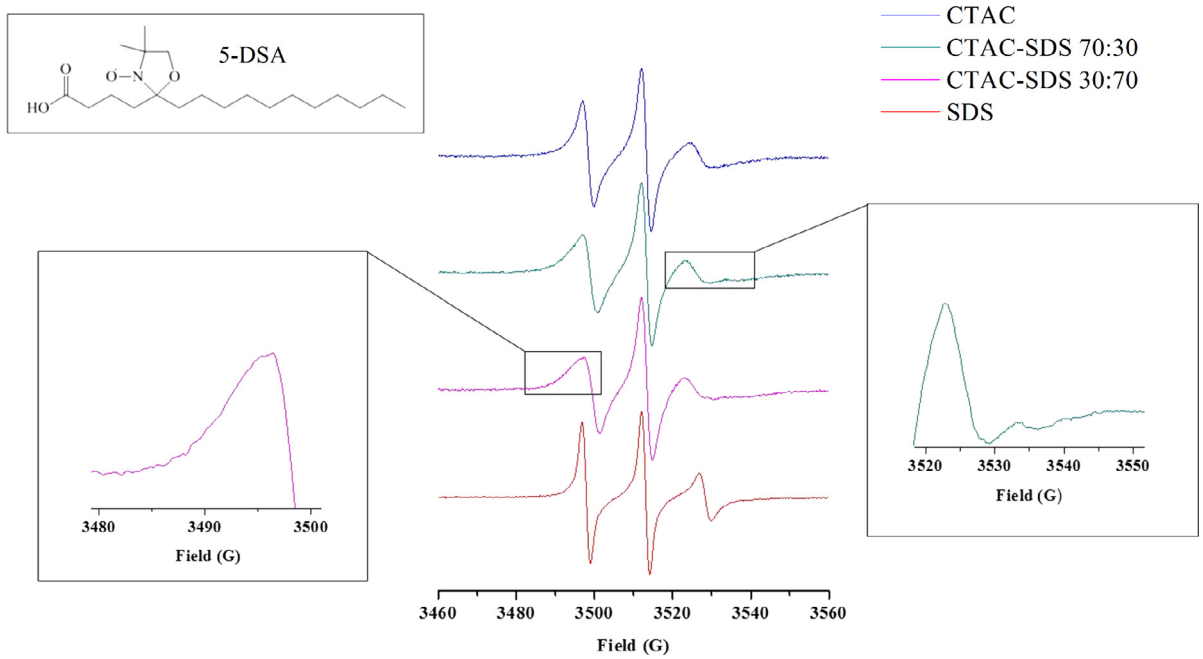

Fig. 4. EPR spectra of 5-DSA in SDS and CTAC aqueous solutions and in mixed surfactant mixtures at total concentration 0.03 mol kg^{-1}. The structure of the spin probe 5-DSA is also shown.

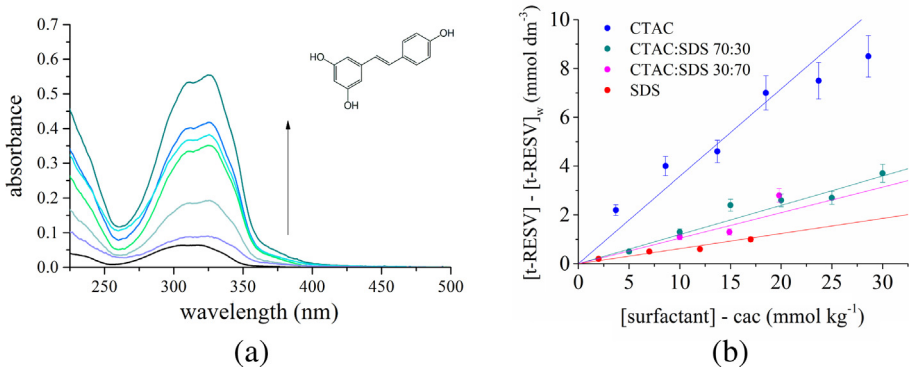

Fig. 5. (a) UV–Vis spectra of *t*-RESV, (whose molecular structure is reported in the inset) in water (black line) and in aqueous mixtures of CTAC-SDS 70:30 with increasing total surfactant concentration from 0.005 to 0.030 mol kg^{-1}. (b) Variation of *t*-RESV concentration in surfactant mixtures with respect to water as a function of the free surfactant concentration in solution. Linear fits of the experimental points used to calculate the molar solubilization capacity, χ, are also shown.

to *cis*-resveratrol occurred nor degradation [69,70]. UV–Vis spectra of *t*-RESV in saturated CTAC-SDS 70:30 solutions at different surfactant concentration, properly diluted after removal of excess solid, are reported in Fig. 5(a). As the surfactant concentration is increased, a significant enhancement of the absorbance is observed, a reflection of the increased chromophore concentration in solution. Similar results were obtained for CTAC and SDS micelles and CTAC-SDS vesicles at different surfactant ratios (data not shown).

With the aim to quantitatively analyze *t*-RESV solubilization by CTAC and/or SDS surfactant mixtures, we determined the molar solubilization capacity, χ. This parameter is defined as the number of moles of *t*-RESV that can be solubilized by one mole of aggregated surfactants [46]. It can be calculated as:

$$\chi = \frac{[t-RESV] - [t-RESV]_w}{[\text{surfactant}] - \text{cac}} \quad (7)$$

where [*t*-RESV] represents the molar concentration of *t*-RESV in the mixture, [*t*-RESV]$_w$ is the maximum solubility of *t*-RESV in water (1.54×10^{-4} M) [71], [surfactant] is the total concentration of the surfactant(s), and cac is the corresponding critical aggregate concentration (for micelles the cmc has been considered).

The values of χ parameter were calculated as the slopes of the ([*t*-RESV] – [*t*-RESV]$_w$) trends versus ([surfactant] – cac), as shown in Fig. 5(b), and are collected in Table 3. Inspection of the figure shows that straight lines satisfactorily fit the data, thus indicating that *t*-RESV is molecularly solubilized in SDS and/or CTAC aggregates, without self-aggregating significantly (e.g. by stacking). *t*-RESV is more efficiently solubilized by cationic than by anionic aggregates, CTAC micelles being more effective than CTAC-SDS 70:30 vesicles. This evidence could indicate cation-π interactions between the *t*-RESV aromatic rings and the cationic headgroups to occur [72,73], thus allowing *t*-RESV to make favorable contacts with the positively charged surface and not only with the hydrophobic portion of the aggregates. These χ values correspond to a high *t*-RESV loading into the catanionic aggregates. Specifically, the values observed for the CTAC-SDS vesicles are almost twice the loading reported for phospholipid-based liposomes [33,74].

By means of fluorescence spectroscopy, we investigated the positioning of *t*-RESV in the solubilizing aggregates. Fluorescence spectra of *t*-RESV are reported in Fig. 6.

An intense composite band centered at 400 nm characterizes the emission spectrum of *t*-RESV in water. Once again, this spectral feature assures that no isomerization to *cis*-resveratrol occurred, since the spectrum of the *cis* isomer is centered at lower wavelengths and is characterized by two well-separated maxima [75]. A significant blue-shift of the emission maximum is observed in all the samples containing surfactant aggregates (see Table 3). However, a comparison with fluorescence spectra of *t*-RESV in different solvents, as reported in the literature [76], allow us to exclude that it is deeply embedded in the aggregate hydrophobic domain, being the observed blue shift much less pronounced than those observed in apolar and aprotic solvents (as an example λ_{max} = 373 nm in ethylacetate) [76]. Thus, we conclude that *t*-RESV remains close to the aggregate interface, partially exposed to water molecules.

3.4. t-RESV radical scavenging capacity

In this work we are interested in monitoring whether *t*-RESV molecules solubilized in CTAC and/or SDS aggregates are able to exert their antioxidant activity in the aqueous environment surrounding micelles/vesicles. The antioxidant activity of phenols is

Table 3
Solubilization features of *t*-RESV in SDS or CTAC micelles and in CTAC-SDS vesicles: molar solubilization capacity (χ) as determined by UV–Vis spectroscopy and emission maximum wavelength (λ_{max}) as determined by fluorescence spectroscopy upon excitation at 318 nm.

	χ	λ_{max} (nm)
SDS	0.06 ± 0.01	387
CTAC	0.36 ± 0.03	387
CTAC-SDS 30:70	0.10 ± 0.01	383
CTAC-SDS 70:30	0.12 ± 0.01	387

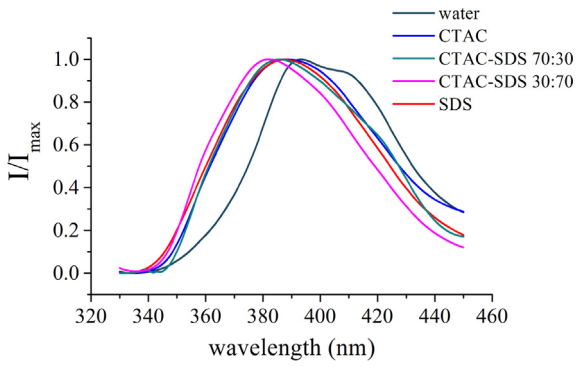

Fig. 6. Normalized fluorescence spectra of *t*-RESV 1.5×10^{-4} M in water and in different aqueous surfactant mixtures at 0.03 mol kg^{-1}.

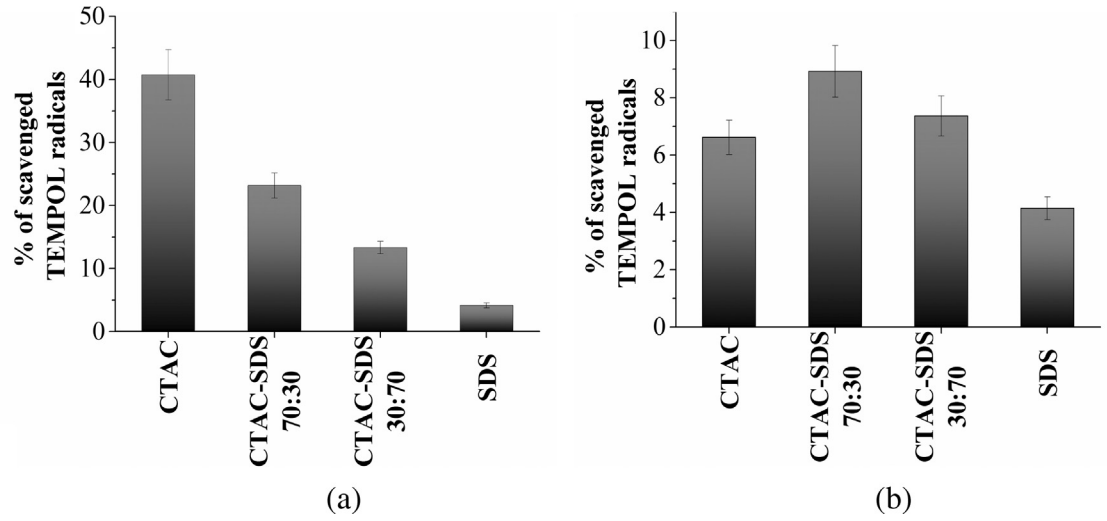

Fig. 7. Percentage of reduction of TEMPOL by saturated solutions of *t*-RESV in the presence of different nano-vehicles at total surfactant concentration 0.03 mol kg^{-1}. The surfactant solutions were saturated with *t*-RESV (a) or contained a constant *t*-RESV concentration (0.0015 mol kg^{-1}, b).

routinely measured by evaluating their reactivity towards a hydrogen-abstracting radical. The most used radical species is DPPH (1,1-diphenyl-2-picrylhydrazyl radical), which requires polar organic solvents, such as dimethyl sulfoxide or ethanol [47], given that its solubility in water is practically nil [77]. However, because of this complex philicity, in microstructured environments, such as surfactant/lipid aggregates, DPPH furnishes equivocal results [78]. An alternative radical easily monitored is the cationic species generated enzymatically from the 2,2′-azino-bis-(3-ethylbenzthiazoline-6-sulfonic acid) ($ABTS^{\bullet+}$) [79]. However, also in this case the presence of an extended aromatic skeleton, joined with the positive charge, could drive specific localization of the probe at the surface of surfactant aggregates, thus reducing the reliability of antioxidant activity tests. Another common test assessing the antioxidant activity, first used to measure the ferric reducing ability of plasma (FRAP), relies on the ferric to ferrous ion reduction at low pH, which causes a colored ferrous-tripyridyltriazine complex to form [80]. However, since multivalent cations tend to condense at the interface of anionic surfactant aggregates [81], and are repelled by cationic aggregates, this method would present evident bias in our case.

For these reasons we had to set up a different method, based on the EPR ability to detect species with unpaired electrons [82], to measure the *t*-RESV radical scavenging activity. In designing the test, our aim was to avoid organic solvents that could heavily affect surfactant self-aggregation and to choose a radical probe soluble in water with low tendency to interact with surfactant aggregates. From this viewpoint TEMPOL was found to be a very suitable choice.

The EPR spectrum of TEMPOL consists of three hyperfine lines (see Supporting Information, Fig. S5) due to the interaction of the unpaired electron with the nitrogen nucleus [83]. In the presence of compounds with antioxidant activity, such as *t*-RESV, the TEMPOL is converted in its reduced form, which is EPR silent. Thus, the scavenging reaction between the free radical and the reducing agent can be followed by monitoring the disappearance of the TEMPOL EPR spectrum [47,48]. Examples of EPR spectra acquired for the different surfactant samples containing *t*-RESV are reported in the ESI. The lineshape of the TEMPOL signal is not affected by the surfactant aggregates in the absence of *t*-RESV. This is a clear evidence that this probe does not interact with the micelles or the vesicles, since in that case a change of a_N and τ_C is expected, which should reflect in a variation of the lines spacing and width [84]. Moreover, the intensity of the TEMPOL signal is not affected by a *t*-RESV suspension prepared in the absence of surfactants, thus indicating that, in order to be effective, *t*-RESV has to be molecularly dispersed. On the other hand, an evident reduction of the TEMPOL signal is observed in mixtures containing the surfactant-solubilized *t*-RESV. Thus, surfactant aggregates solubilize *t*-RESV and at the same time leave it sufficiently exposed to the aqueous medium so that it can effectively scavenge the radical.

The percentage of scavenged TEMPOL, calculated for all *t*-RESV-surfactant samples as well as for the control *t*-RESV aqueous solution as described in the experimental section, is reported in Fig. 7.

Overall, the radical scavenging capability is quite satisfactory, especially considering that we added no co-solvent or additional solubilizer to the surfactant aqueous mixture of interest. The capability of *t*-RESV as radical scavenger clearly depends on its concentration. Indeed, its low solubility in water hampers its action in this medium. If the results obtained for the samples in which the surfactant aggregates are saturated with *t*-RESV are considered (Fig. 7(a)) it is evident that scavenging effect increases with increasing *t*-RESV solubility, so that the highest effect is obtained for CTAC micelles and the lowest for SDS micelles. However, solubility is not the only important factor to determine *t*-RESV antioxidant activity. Indeed, analyzing the effects of the surfactant samples with the same *t*-RESV concentration (Fig. 7(b)), it appears that vesicular mixtures perform better than micellar ones. Particularly, CTAC-SDS 70:30 is the surfactant mixture for which the best *t*-RESV scavenging activity is obtained. This could be connected to the better structuring of surfactant molecules in bilayered structures with respect to micellar ones. The more ordered bilayer interphase with the aqueous medium provides a more favorable environment for the reaction between the scavenging polyphenol and the radical species.

4. Conclusions

By a combined experimental strategy including DLS, ELS, SANS, EPR, UV and fluorescence spectroscopies, we have analyzed and rationalized the functional behavior of CTAC-SDS aqueous mixtures in terms of their microstructure and dynamics. Indeed, this system presents an extremely large range of composition in which only cationic-rich vesicles form. This range is much wider than that

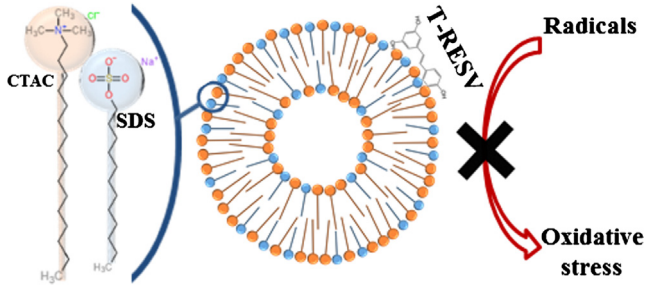

Fig. 8. Schematic representation of the mechanism underlying the radical scavenging activity of *t*-RESV solubilized in CTAC-SDS catanionic vesicles.

observed for the CTAB-SDS mixtures that, besides vesicles, tend to form elongated micelles [85,86]. Thus, vesicle stabilization can be ascribed to an indirect effect of the chloride ions, which destabilize micellar aggregates with high surface curvature, thus favoring bilayered structures.

The relevance of the counterion nature in the self-aggregation behavior of catanionic surfactant mixture has been for long underestimated, or considered to be effective only in the presence of added electrolyte at high concentration [87,52,24]. Our results query this common belief, highlighting the need of a reconsideration of the current state of understanding of catanionic mixture behavior focusing on the molecular buildup of the aggregates [88].

Because of the asymmetry between the alkyl tails of the two surfactants, a partial interdigitation of their termini in the bilayer inner core occurs, further stabilizing the aggregate, whose microstructural properties are poorly affected by changes in surfactant composition and total surfactant concentration.

CTAC-SDS catanionic vesicles are optimal nano-vehicles for the solubilization and delivery of actives, as we demonstrated using the natural polyphenol *t*-RESV. The loading of this aromatic poorly water-soluble species in CTAC-SDS aggregates is among the highest reported in the literature [89–93].

Most importantly, *t*-RESV is molecularly solubilized among the surfactant headgroups, remaining partially exposed to the surrounding environment, without undergoing to any isomerization or self-aggregation process. Consistently, it exerts a significant scavenging activity towards radicals in aqueous media (see the sketch in Fig. 8), as estimated by a test designed to reliably monitor antioxidant activity in the presence of surfactant aggregates. Indeed, percentages of scavenged radicals detected for CTAC-SDS aggregates are comparable, and in some cases higher than those reported in recent literature for more sophisticated delivery systems [74,93–97].

Besides the interest for the fundamental understanding of the catanionic mixture behavior and of the solubilization process in these systems, our results also present an evident applicative relevance.

Notwithstanding their unique physico-chemical properties, the industrial exploitation of catanionic vesicles remains quite limited. As widely recognized, they present a good potential as drug delivery systems [15–17,98,99]. However, most of the studies in this field concern surfactants of scarce, if any, use in the formulative practice. CTAC, or similar alkyl ammonium chlorides, are massively used in the formulations of conditioners, softeners and sanitizers. At the same time, SDS is representative of the anionic surfactants commonly used as detergents. Both surfactants are accepted for the topical use on the skin as well as on hairs. Consequently, the present study paves the way to the design of new surfactant-based products to which active solubilization provides substantial added value.

Conflict of interest

The authors declare no competing financial interest.

Acknowledgements

Dr. Richard Heenan and Dr. Aurel Radulescu are kindly acknowledged for their technical assistance in neutron collection data at LOQ diffractometer at ISIS Pulsed Neutron Source (Science and Technology Facilities Council, Rutherford Appleton Laboratory, Didcot - UK) and at KWS2 instrument at the Heinz Meier Leibtnitz Source, Garching Forschungszentrum (Germany).

Appendix A. Supplementary material

Supplementary data associated with this article can be found, in the online version, at http://dx.doi.org/10.1016/j.jcis.2017.04.032.

References

[1] J.C. Hao, H. Hoffmann, Curr. Opin. Colloid Interface Sci. 9 (2004) 279–293.
[2] H.T. Jung, B. Coldren, J.A. Zasadzinski, D.J. Iampietro, E.W. Kaler, Proc. Natl. Acad. Sci. USA 98 (2001) 1353–1357.
[3] E.W. Kaler, K.L. Herrington, A.K. Murthy, J.A.N. Zasadzinski, J. Phys. Chem. 96 (1992) 6698–6707.
[4] A. Khan, E.F. Marques, Curr. Opin. Colloid Interface Sci. 4 (1999) 402–410.
[5] E.F. Marques, O. Regev, A. Khan, B. Lindman, Adv. Colloid Interface Sci. 100 (2003) 83–104.
[6] S. Segota, D. Tezak, Adv. Colloid Interface Sci. 121 (2006) 51–75.
[7] S.G. Silva, M.L.C. do Vale, E.F. Marques, Chem.-Eur. J. 21 (2015) 4092–4101.
[8] B.F.B. Silva, E.F. Marques, U. Olsson, R. Pons, Langmuir 26 (2010) 3058–3066.
[9] E. Nabi, M. Drechsler, M. Gradzielski, Colloid Polym. Sci. 293 (2015) 3119–3130.
[10] N. Manghisi, C. Leggio, A. Jover, F. Meijide, N.V. Pavel, V.H.S. Tellini, J.V. Tato, R. G. Agostino, L. Galantini, Angew. Chem. Int. Ed. 49 (2010) 6604–6607.
[11] Y.M. Li, H.X. Zhang, Z.N. Wang, M.T. Bao, Colloid Polym. Sci. 292 (2014) 2349–2360.
[12] P. Koshy, V.K. Aswal, M. Venkatesh, P.A. Hassan, J. Phys. Chem. B 115 (2011) 10817–10825.
[13] H.Q. Yin, Y.Y. Lin, J.B. Huang, J. Colloid Interface Sci. 338 (2009) 177–183.
[14] M. Gradzielski, J. Phys. Condens. Matter 15 (2003) R655–R697.
[15] Y. Jiang, F.F. Li, Y.X. Luan, W.T. Cao, X.Q. Ji, L.X. Zhao, L.L. Zhang, Z.H. Li, Int. J. Pharm. 436 (2012) 806–814.
[16] C. Pucci, A. Scipioni, M. Diociaiuti, C. La Mesa, L. Perez, R. Pons, RSC Adv. 5 (2015) 81168–81175.
[17] S. Ghosh, A. Ray, N. Pramanik, B. Ambade, C. R. Chim. 19 (2016) 951–954.
[18] C.G. Ferguson, R.D. James, C.S. Bigman, D.A. Shepard, Y. Abdiche, P.S. Katsamba, D.G. Myszka, G.D. Prestwich, Bioconjugate Chem. 16 (2005) 1475–1483.
[19] E.F. Marques, Langmuir 16 (2000) 4798–4807.
[20] P.A. Hassan, T.K. Hodgdon, M. Sagasaki, G. Fritz-Popovski, E.W. Kaler, C. R. Chim. 12 (2009) 18–29.
[21] M.T. Yatcilla, K.L. Herrington, L.L. Brasher, E.W. Kaler, S. Chiruvolu, J.A. Zasadzinski, J. Phys. Chem. 100 (1996) 5874–5879.
[22] M. Bergstrom, J.S. Pedersen, J. Phys. Chem. 104 (2000) 4155–4163.
[23] E. Marques, A. Khan, M.D. Miguel, B. Lindman, J. Phys. Chem. 97 (1993) 4729–4736.
[24] S. Prevost, M. Gradzielski, J. Colloid Interface Sci. 337 (2009) 472–484.
[25] P. Wang, Y.Y. Ma, Z.B. Liu, Y.G. Yan, X.L. Sun, J. Zhang, RSC Adv. 6 (2016) 13442–13449.
[26] D.S. Murphy, J. Surfactants Deterg. 18 (2015) 199–204.
[27] U. Tezel, S.G. Pavlostathis, Curr. Opin. Biotech. 33 (2015) 296–304.
[28] V.S. Kadam, A.G. Chintale, K.P. Deshmukh, D.N. Nalwad, Int. J. Res. Pharm. Chem. 3 (2013) 308–316.
[29] F. Orallo, Curr. Med. Chem. 15 (19) (2008) 1887–1898.
[30] C.A. de la Lastral, I. Villegas, Biochem. Soc. Trans. 35 (2007) 1156–1160.
[31] M. Atanackovic, M. Posa, H. Heinle, L. Gojkovic-Bukarica, J. Cvejic, Colloids Surf. B 72 (2009) 148–154.
[32] G. Davidov-Pardo, D.J. McClements, Trends Food Sci. Tech. 38 (2014) 88–103.
[33] B.D. Isailovic, I.T. Kostic, A. Zvonar, V.B. Dordevic, M. Gasperlin, V.A. Nedovic, B. M. Bugarski, Innov. Food Sci. Emerg. Technol. 19 (2013) 181–189.
[34] Z. Lu, B. Cheng, Y.L. Hu, Y.H. Zhang, G.L. Zou, Food Chem. 113 (2009) 17–20.
[35] U.M. Musazzi, I. Youm, J.B. Murowchick, M.J. Ezoulin, B.B.C. Youan, Colloids Surf. B 118 (2014) 234–242.
[36] A. Lomakin, D.B. Teplow, G.B. Benedek, Quasielastic Light Scattering for Protein Assembly Studies, in: E.M. Sigurdsson (Ed.), Amyloid Proteins: Methods And Protocols, vol. 299, Humana Press, Totowa, New Jearsey, 2005.
[37] H.X. Zhang, O. Annunziata, J. Phys. Chem. B 112 (2008) 3633–3643.
[38] R.K. Heenan, J. Penfold, S.M. King, J. Appl. Crystallogr. 30 (1997) 1140–1147.
[39] A. Radulescu, V. Pipich, H. Frielinghaus, M.S. Appavou, J. Phys. Conf. Ser. 351 (2012).

[40] P. Bartlett, R.H. Ottewill, J. Chem. Phys. 96 (1992) 3306–3318.
[41] T.P. Russell, J.S. Lin, S. Spooner, G.D. Wignall, J. Appl. Crystallogr. 21 (1988) 629–638.
[42] J.H. Freed, Theory of slow tumbling ESR spectra for nitroxides, in: L.J. Berliner (Ed.), Spin Labeling Theory and Applications, Academic Press, New York, 1976, pp. 53–132.
[43] R. Pogni, G. Della Lunga, E. Busi, R. Basosi, Int. J. Quantum Chem. 73 (1999) 249–254.
[44] E. Busi, G. Vitiello, M. Niccoli, R. Basosi, D. Montesarchio, G. D'Errico, Biochim. Biophys. Acta-Biomembr. 1828 (2013) 2074–2082.
[45] A.M. Tedeschi, E. Busi, R. Basosi, L. Paduano, G. D'Errico, J. Solution Chem. 35 (2006) 951–968.
[46] C.O. Rangel-Yagui, A. Pessoa, L.C. Tavares, J. Pharm. Pharm. Sci. 8 (2005) 147–163.
[47] M. Polovka, V. Brezova, A. Stasko, Biophys. Chem. 106 (2003) 39–56.
[48] E.D. Tzika, V. Papadimitriou, T.G. Sotiroudis, A. Xenakis, Food Biophys. 3 (2008) 48–53.
[49] A.M. Khan, S.S. Shah, J. Chem. Soc. Pak. 30 (2008) 186–191.
[50] L. Tofani, A. Feis, R.E. Snoke, D. Berti, P. Baglioni, G. Smulevich, Biophys. J. 87 (2004) 1186–1195.
[51] G. Vitiello, G. Mangiapia, E. Romano, M. Lavorgna, S. Guido, V. Guida, L. Paduano, G. D'Errico, Colloids Surf. A 442 (2014) 16–24.
[52] N. Vlachy, M. Drechsler, D. Touraud, W. Kunz, C. R. Chim. 12 (2009) 30–37.
[53] A. Di Michele, L. Brinchi, P. Di Profio, R. Germani, G. Savelli, G. Onori, J. Colloid Interface Sci. 358 (2011) 160–166.
[54] J.B. Hayter, J. Penfold, Mol. Phys. 42 (1981) 109–118.
[55] V.K. Aswal, P.S. Goyal, Phys. B 245 (1998) 73–80.
[56] V.K. Aswal, P.S. Goyal, Phys. Rev. E 61 (2000) 2947–2953.
[57] V.K. Aswal, J. Kohlbrecher, P.S. Goyal, H. Amenitsch, S. Bernstorff, J. Phys. Condens. Matter 18 (2006) 11399–11410.
[58] J.S. Higgins, H. Benoit, Polymers and Neutron Scattering, Clarendon, Oxford, 1994.
[59] J. Berghausen, J. Zipfel, P. Lindner, W. Richtering, J. Phys. Chem. B 105 (2001). 11081–11088.
[60] G. Del Re, G. D'Errico, O. Ortona, V. Vitagliano, J. Colloid Interface Sci. 349 (2010) 230–235.
[61] N. Ruocco, H. Frielinghaus, G. Vitiello, G. D'Errico, L.G. Leal, D. Richter, O. Ortona, L. Paduano, J. Colloid Interface Sci. 452 (2015) 160–168.
[62] E. Szajdzinskapietek, R. Maldonado, L. Kevan, R.R.M. Jones, J. Am. Chem. Soc. 107 (1985) 6467–6470.
[63] M. Grimaldi, M. Scrima, C. Esposito, G. Vitiello, A. Ramunno, V. Limongelli, G. D'Errico, E. Novellino, A.M. D'Ursi, Biochim. Biophys. Acta-Biomembr. 1798 (2010) 660–671.
[64] D.D. Neto, C.E.G. Salmon, A. Alonso, M. Tabak, Colloids Surf. B 70 (2009) 147–156.
[65] P.S. Santiago, D.D. Neto, L.R.S. Barbosa, R. Itri, M. Tabak, J. Colloid Interface Sci. 316 (2007) 730–740.
[66] G. Vitiello, A. Falanga, A.A. Petruk, A. Merlino, G. Fragneto, L. Paduano, S. Galdiero, G. D'Errico, Soft Matter 11 (2015) 3003–3016.
[67] L. Ciani, S. Ristori, L. Calamai, G. Martini, Biochim. Biophys. Acta-Biomembr. 1664 (2004) 70–79.
[68] A. Guder, H. Korkmaz, H. Gokce, Y.B. Alpaslan, G. Alpaslan, Spectrochim. Acta A 133 (2014) 378–395.
[69] T.S. Figueiras, M.T. Neves-Petersen, S.B. Petersen, J. Fluoresc. 21 (2011) 1897–1906.
[70] S. Zupancic, Z. Lavric, J. Kristl, Eur. J. Pharm. Biopharm. 93 (2015) 196–204.
[71] Y.L. Jiang, Bioorg. Med. Chem. 16 (2008) 6406–6414.
[72] K.S. Kim, J.Y. Lee, S.J. Lee, T.K. Ha, D.H. Kim, J. Am. Chem. Soc. 116 (1994) 7399–7400.
[73] A.R. Tehrani-Bagha, R.G. Singh, K. Holmberg, J. Colloid Interface Sci. 376 (2012) 112–118.
[74] C. Caddeo, M. Manconi, A.M. Fadda, F. Lai, S. Lampis, O. Diez-Sales, C. Sinico, Colloids Surf. B 111 (2013) 327–332.
[75] A. Amri, J.C. Chaumeil, S. Sfar, C. Charrueau, J. Control. Release 158 (2012) 182–193.
[76] S. Bellow, G. Latouche, S.C. Brown, A. Poutaraud, Z.G. Cerovic, J. Exp. Bot. 63 (2012) 3697–3707.
[77] M.C. Foti, J. Agric. Food Chem. 63 (2015) 8765–8776.
[78] C. Aliaga, M.C. Rezende, A. Arenas, Food Chem. 113 (2009) 1083–1087.
[79] M.B. Arnao, A. Cano, M. Acosta, Food Chem. 73 (2001) 239–244.
[80] I.F.F. Benzie, J.J. Strain, Anal. Biochem. 239 (1996) 70–76.
[81] H. Xu, J. Penfold, R.K. Thomas, J.T. Petkov, I. Tucker, J.R.P. Webster, I. Grillo, A. Terry, Langmuir 30 (2014) 4694–4702.
[82] A.B. Muñoz-García, F. Sannino, G. Vitiello, D. Pirozzi, L. Minieri, A. Aronne, P. Pernice, M. Pavone, G. D'Errico, A.C.S. Appl, Mater. Interfaces 7 (2015) 21662–21667.
[83] N.D. Yordanov, K. Ranguelova, Spectrochim. Acta A 56 (2000) 373–378.
[84] A.M. Tedeschi, G. D'Errico, E. Busi, R. Basosi, V. Barone, Phys. Chem. Chem. Phys. 4 (2002) 2180–2188.
[85] B. Tah, P. Pal, M. Mahato, G.B. Talapatra, J. Phys. Chem. B 115 (2011) 8493–8499.
[86] B. Sohrabi, H. Gharibi, S. Javadian, M. Hashemianzadeh, J. Phys. Chem. B 111 (2007) 10069–10078.
[87] L. Chen, H. Xing, P. Yan, J.-M. Maa, J.-X. Xiao, Soft Matter 7 (2011) 5365–5372.
[88] L. Chiappisi, H. Yalcinkaya, V.K. Gopalakrishnan, M. Gradzielski, T. Zemb, Colloid Polym. Sci. 293 (2015) 3131–3143.
[89] M. Lee, C.G. Park, B.K. Huh, Se-Na Kim, S.H. Lee, R. Khalmuratova, J.-W. Park, H.-W. Shin, Y.B. Choy, Sci. Rep. 7 (2017) 40249.
[90] M.R. Vijayakumar, R. Kosuru, S.K. Singh, C.B. Prasad, G. Narayan, M.S. Muthu, S. Singh, RSC Adv. 6 (2016) 74254–74268.
[91] B. Balanč, K. Trifković, V. Đorđević, S. Marković, Rada Pjanović, Viktor Nedović, B. Bugarski, Food Hydrocolloids 61 (2016) 832–842.
[92] D. Pando, M. Matos, G. Gutiérrez, C. Pazos, Colloids Surf. B 128 (2015) 398–404.
[93] I. Scognamiglio, D. De Stefano, V. Campani, L. Mayol, R. Carnuccio, G. Fabbrocini, F. Ayala, M.I. La Rotonda, G. De Rosa, Int. J. Pharm. 440 (2013) 179–187.
[94] W. Wang, Q. Tang, T. Yu, X. Li, Y. Gao, J. Li, Y. Liu, L. Rong, Z. Wang, H. Sun, H. Zhang, B. Yang, A.C.S. Appl, Mater. Interfaces 9 (2017) 3376–3387.
[95] Y. Zu, Y. Zhang, W. Wang, X. Zhao, X. Han, K. Wang, Y. Ge, Drug Deliv. 23 (2016) 971–981.
[96] X. Huang, Y. Dai, J. Cai, N. Zhong, H. Xiao, D. Julian, McClements, K. Hu, Food Hydrocolloids 64 (2017) 157–165.
[97] R. Pangeni, S. Sharma, G. Mustafa, J. Ali, S. Baboota, Nanotechnology 25 (2014) 485102.
[98] S. Geng, Y. Wang, L. Wang, T. Kouyama, T. Gotoh, S. Wada, J.-Y. Wang, Sci. Rep. 7 (2017) 39202.
[99] S. Li, C. Fang, J. Zhang, B. Liu, Z. Wei, X. Fan, Z. Sui, Q. Tan, Nanomedicine 12 (2016) 1567–1579.